AD NUMBER

AD819344

LIMITATION CHANGES

TO:

Approved for public release; distribution is unlimited.

FROM:

**Distribution authorized to U.S. Gov't. agencies and their contractors;
Administrative/Operational Use; JUL 1967. Other requests shall be referred to Air Force Avionics Lab., Wright-Patterson AFB, OH 45433.**

AUTHORITY

AFWAL ltr 28 Jan 1988

AN EXPERIMENT TO DETERMINE THE MAGNITUDE AND FREQUENCY CHARACTERISTICS OF ATMOSPHERIC SHIMME OBSERVED FROM HIGH ALTITUDE AIRCRAFT

LOWELL TECHNOLOGICAL INSTITUTE

RESEARCH FOUNDATION

LOWELL, MASSACHUSETTS

LTIRF-268/RP
(Vol. 2 of 2)

LOWELL TECHNOLOGICAL INSTITUTE RESEARCH FOUNDATION
Lowell, Massachusetts

AN EXPERIMENT TO DETERMINE THE MAGNITUDE AND FREQUENCY CHARACTERISTICS OF ATMOSPHERIC SHIMMER OBSERVED FROM HIGH ALTITUDE AIRCRAFT

Contract No. F33615-67-C-1136

ARPA Order No. 449, Amendment 4, Task 5

Program Code No. 6E30

Final Technical Report

July 1967

Prepared for

Air Force Avionics Laboratory, AVRO
Research and Technology Division
Air Force Systems Command
United States Air Force
Wright-Patterson Air Force Base, Ohio

TABLE OF CONTENTS

TABLE OF CONTENTS
(cont'd)

1.0 INTRODUCTION

Recent investigations of the tracking capability of infrared airborne tracking systems indicate that their precision is approaching the point where atmospheric effects must be taken into account if further improvement is to be accomplished. The tracking systems considered are those designed to detect and lock onto a target, and, by utilizing servo systems, to position other optical measuring instruments on the same target.

Two types of errors caused by the atmosphere are present. One is a static positioning error caused by atmospheric refraction which displaces the apparent target position from the true position. The magnitude and direction of this error can change with time, but, if these changes are of long duration with respect to the tracker frequency response, no pointing errors will be imparted to the slaved measuring instruments; these changes need only be considered when the true direction of the target is required. The second type of error, to which we address our attention in this report, results from fluctuations in the apparent position of the target at angular rates beyond the ability of a tracker to follow, thus causing pointing errors of the slaved instruments with respect to the apparent target position which are equal in magnitude to the fluctuations. In the case of photography, for example, this causes blurring of the image.

This angular fluctuation is known as shimmer, and is due primarily to the motion of turbulent air passing across the line

of sight, which causes a variation in the refractive index, and consequently, a bending of the path to the observer.

When two sources are sufficiently close in angular position, their apparent motions will be partially correlated. Uncorrelated motion, known as differential shimmer, causes image distortion. The degree of correlation in the shimmer decreases as the angular separation of two sources increases.

This report proposes an experiment which will measure the magnitude and frequency of shimmer at the altitudes and distances that airborne trackers typically use to observe reentry events. The experiment will also yield information on the percent correlation in the shimmer movements of objects at a series of small angular separations. This will be accomplished by utilizing two aircraft, one carrying high intensity light sources to be used as a target, and the other carrying high resolution, fast framing cameras which will photograph these sources and thus will record their apparent angular movements. The aircraft will always be flown on parallel courses; they should be flown at a variety of altitude, speed, and range configurations to investigate the effect of these parameters on the magnitude and frequency of shimmer. The shimmer measurements described in this report will serve to increase our knowledge of the ultimate limits of resolution obtainable by airborne, tracker oriented, optical instruments, and will provide data useful in the specification and design of future tracker systems.

2.0 EXPERIMENTAL OBJECTIVES AND CONCEPTS

The objective of the proposed experiment is to obtain data concerning the effects of atmospheric shimmer on airborne tracking capability. In particular, we are concerned with the ability of the tracker to follow the fluctuations in the apparent position of the target, so as to prevent a loss of resolution in the imaging process. There is considerable need for such an experiment, because presently available data is based on ground observations, and is of questionable value when extrapolated to the airborne environment.

In a later section of this report (Section 4.0), we discuss the theoretical problem, and indicate how we might go about deducing information about the shimmer process, with the ultimate objective of eventually being able to predict the effect of shimmer under various conditions and at various altitudes. But there appears to be little practical value in making theoretical predictions without actual data based on the real airborne tracker environment. We therefore now address ourselves to the problem of obtaining such information.

2.1 Statement of the Problem and Mathematical Background

Let us consider a camera observing a point source of light at a particular range and altitude, without any relative motion between observer and source. Suppose we were to measure

the angular fluctuations of the apparent position of the light source from its mean position, as a function of time, due to atmospheric shimmer. Suppose also that we were to develop a voltage proportional to this deviation in position (in a particular direction), to amplify this voltage, and then to employ it in driving a servo motor which could point the camera platform in such a direction as to reduce this deflection, thereby avoiding the smearing of the optical image. The questions we wish to be able to answer for observations at various altitudes, ranges, and conditions of observation are:

(a) What frequency characteristics of the servo system would be required to enable a particular tracker to follow the fluctuations in the apparent image position without photographic smearing due to image "dancing"? In other words, what frequencies would be present in what proportions in the driving signal? [This signal would be represented by the open-loop voltage seen at the input of the amplifier with the servo motor disengaged from the platform.]

(b) What is the average power required of the servo system in order to overcome the effect of atmospheric shimmer?

(c) Since we have the need of resolving the image of a target of finite extent, and since our resolution is also degraded by relative motion of various elements of the image with respect to each other, what are the

frequency characteristics of the relative motion of two sources of light due to atmospheric shimmer, as a function of angular displacement? [Although this degradation cannot be relieved by the tracking system, it may introduce a fundamental limitation in resolution capability which can affect the design of the tracker.]

(d) To what extent is atmospheric shimmer primarily a result of local aircraft-induced turbulence, and hence a function of the aerodynamics of the aircraft and the location of the camera? And, to what extent is it rather the result of independent atmospheric agitation?

We now briefly review the required mathematical formalism. Let a(t) be the angular deflection of the apparent image from its mean position (or, alternately, it may be thought of as the voltage proportional to this deflection). Then $|a(t)|^2$ is, except for a constant of proportionality, a measure of the signal power required to drive the servo. If a(t) were a periodic function, its Fourier representation could be written in complex form

$$a(t) = \sum_{n=-\infty}^{\infty} A_n e^{i(2n\pi t/T)} \quad , \qquad (1)$$

where

T is the period, and the Fourier coefficients are

$$A_n = \frac{1}{T} \int_{-\frac{T}{2}}^{+\frac{T}{2}} a(t)e^{-i(2n\pi t/T)}dt \quad . \tag{2}$$

Since, however, a(t) is a non-periodic function, we obtain its Fourier representation by letting $T \to \infty$. The fundamental Fourier frequency then decreases and the discrete harmonics move closer together, until in the limit the series of Equation (1) becomes an integral, and the discrete complex Fourier amplitudes A_n of Equation (2) become a continuous spectrum $A(\omega)$. This spectrum is of course called the Fourier transform of a(t), which is defined with a convenient constant factor as

$$A(\omega) = \frac{1}{2\pi} \int_{-\infty}^{\infty} a(t)e^{-i\omega t}dt \quad . \tag{3}$$

In the same limit, Equation (1) is replaced by the inverse Fourier transform relationship

$$a(t) = \int_{-\infty}^{\infty} A(\omega)e^{i\omega t}d\omega \quad . \tag{4}$$

We now introduce an integral defined as

$$\phi(\tau) = \int_{-\infty}^{\infty} a(t)a(t + \tau)dt \quad . \tag{5}$$

Then it can be proven [2-1] that, if $\Phi(\omega)$ is the Fourier Transform of $\phi(\tau)$, i.e., if it is defined by

$$\Phi(\omega) = \frac{1}{2\pi} \int_{-\infty}^{\infty} \phi(\tau) e^{-i\omega\tau} d\tau \quad , \tag{6}$$

then this transform is related to $A(\omega)$, the transform of $a(t)$, by

$$\Phi(\omega) = 2\pi |A(\omega)|^2 \quad . \tag{7}$$

We call $\phi(\tau)$ the autocorrelation function of the real function $a(t)$. Since, however, $a(t)$ is really a random function due to the stochastic nature of atmospheric shimmer, then, to be more rigorous, we should redefine $\phi(\tau)$ in terms of a sequence of measurements, i.e.,

$$\phi_{aa}(\tau) = \lim_{T\to\infty} \frac{1}{2T} \int_{-T}^{T} a(t)a(t+\tau)dt \quad . \tag{8}$$

We can see the physical significance of this function by observing from Equation (8) that

$$\phi_{aa}(0) = \lim_{T\to\infty} \frac{1}{2T} \int_{-T}^{T} [a(t)]^2 dt \quad , \tag{9}$$

which is simply the mean square value of the atmospheric shimmer; its knowledge enables one to determine the average power required of a servo system to drive a tracker in overcoming the effect of shimmer in the apparent position of a point target.

But if we now consider the Fourier transform of $\phi_{aa}(\tau)$, namely,

$$\Phi_{aa}(\omega) = \frac{1}{2\pi} \int_{-\infty}^{\infty} \phi_{aa}(\tau) e^{-i\omega\tau} d\tau \quad , \tag{10}$$

then from the inverse Fourier relationship analogous to Equation (4), it follows that

$$\phi_{aa}(0) = \int_{-\infty}^{\infty} \Phi_{aa}(\omega) d\omega \quad . \tag{11}$$

Thus the mean square signal power may be obtained by integrating $\Phi_{aa}(\omega)$ over all frequencies. Hence we call $\Phi_{aa}(\omega)$ the power density spectrum of the signal a(t). Equation (10) states that the power density spectrum is the Fourier transform of the autocorrelation function of a(t). Equation (7) enables us to determine $|A(\omega)|$, thus obtaining the relative magnitude of atmospheric fluctuation present at any given frequency.

Therefore, if we can measure the autocorrelation function of the atmospheric shimmer, its value at zero argument gives us the mean square shimmer power, and its Fourier transform enables us to establish its frequency characteristics.

We shall also have use for the crosscorrelation of two real functions a(t) and b(t), namely,

$$\phi_{ab}(\tau) = \lim_{T\to\infty} \frac{1}{2T} \int_{-T}^{T} a(t)b(t+\tau)dt. \tag{12}$$

It may be seen that for two completely independent random signals the crosscorrelation function vanishes identically. The cross-correlation function likewise has its Fourier transform $\Phi_{ab}(\omega)$, and may similarly be shown to be related to the transforms of a(t) and b(t) by

$$\Phi_{ab}(\omega) = A(\omega)*B(\omega) \ , \qquad (13)$$

where the asterisk indicates complex conjugate.

2.2 Measurement Process

We have defined our problem in terms of measuring the autocorrelation function of the angular deflection of a point source from its mean position, due to atmospheric shimmer. In order to accomplish this, we must eliminate image motion due to other effects, such as aircraft vibration. Moreover, if we are trying to determine how much of the shimmer is due to independent atmospheric turbulence, as opposed to aircraft induced turbulence, we would like to have the means of eliminating the effect of the latter.

The target aircraft will fly a course parallel to the observer aircraft, and at the same speed. The target will consist of a series of five reference lights in a line to be used as point sources. Two cameras mounted at different aircraft stations will produce, for a given run, one second of high-speed film data (400 frames/sec). Each frame contains the images of the five

reference lights, of a reference fiducial which gives a fixed position relative to the camera coordinates, and the time of measurement. The displacement of each of the reference light images relative to the reference fiducial will be measured by means of a microdensitometer.

2.2.1 Independent Atmospheric Shimmer

We now consider the determination of that portion of the shimmer whose presence is independent of the disturbance induced by the aircraft. Clearly, this type of shimmer will always be present and is not affected by the choice of aircraft or the camera station in the aircraft.

We have stated in Section 2.1 that the shimmer spectrum may be completely constructed from the displacement of the image of a light source from its mean position, and, in particular, from the autocorrelation function of this displacement. In other words, we can generate the function $\phi_{aa}(\tau)$ of Equation (8) by forming and integrating products of the angular displacements $a(t)$ and $a(t+\tau)$ of a light image from its average position, obtained from all pairs of picture frames separated by a time interval τ; this calculation is, of course, repeated for all τ. The mean square value of the shimmer is simply $\phi_{aa}(0)$, and the magnitude of the shimmer spectrum $|A(\omega)|$ is obtained by Fourier transforming $\phi_{aa}(\tau)$, and then using Equation (7).

However, this shimmer data would necessarily include aircraft induced turbulence, as well as any residual aircraft

vibration effects which may not have been completely uncoupled from the camera. In the course of obtaining this data, we actually measure the position of the image of the light source with respect to the fiducial, since, a priori, we do not know the mean position of the source. We could then process the data to obtain the mean position and make the necessary coordinate transformation. But if instead we difference the angular displacements of two different light sources measured from the fiducial, then it is possible to separate out completely the effects of both aircraft induced turbulence and vibration. Intuitively it is obvious that such local disturbances will affect the motion of the images of the two light sources identically, and that when we take the difference we separate out these local effects. We will now prove that the shimmer spectrum obtained from this so-called "differential shimmer" of two images as measured from source to source is in fact identical to the spectrum of the shimmer of one of the images with respect to its average position, provided only that the angular spacing of the two sources is larger than the correlation angle.

If we designate the apparent angular displacement of one of the sources with respect to its average position as a(t), and the other as b(t), then the autocorrelation function of either of them is equal to that of the other, assuming that the light rays travel through turbulence possessing the same statistical properties.

Thus

$$\phi_{aa}(\tau) = \lim_{T\to\infty} \frac{1}{2T} \int_{-T}^{T} a(t)a(t+\tau)dt = \phi_{bb}(\tau) \ .$$

Actually, of course, what we measure is $a_f(t)$, the image position with respect to the fiducial, where

$$a(t) = a_f(t) - \overline{a_f(t)} \equiv a_f(t) - \overline{a_f} \ ,$$

with $\overline{a_f}$ being the location of the average position with respect to the fiducial.

What is convenient to compute from the film data is the autocorrelation function of $a_f(t)$, namely

$$\phi_{a_f a_f}(\tau) = \lim_{T\to\infty} \frac{1}{2T} \int_{-T}^{T} [a(t)+\overline{a_f}][a(t+\tau)+\overline{a_f}]dt$$

$$= \lim_{T\to\infty} \left[\frac{1}{2T} \int_{-T}^{T} a(t)a(t+\tau)dt + \frac{\overline{a_f}}{2T} \int_{-T}^{T} a(t)dt \right.$$

$$\left. + \frac{\overline{a_f}}{2T} \int_{-T}^{T} a(t+\tau)dt + \frac{\overline{a_f}^2}{2T} \int_{-T}^{T} dt \right] \ .$$

Thus,

$$\phi_{a_f a_f}(\tau) = \phi_{aa}(\tau) + 2\overline{a}_f\overline{a(t)} + \overline{a_f}^2 = \phi_{aa}(\tau) + \overline{a_f}^2 \ , \quad (14)$$

since $\overline{a(t)}$, the average value of a(t), vanishes by definition.

Clearly, the Fourier spectrum of $\phi_{a_f a_f}(\tau)$ is the same as that of $\phi_{aa}(\tau)$, except for a Dirac delta function (unit impulse) $\delta(\omega)$ at zero frequency due to the $\overline{a_f}^2$ term. However, we need to compute $\overline{a_f}$ if we wish to obtain the mean square value of the shimmer $\phi_{aa}(0)$ from $\phi_{a_f a_f}(0)$.

On the other hand, the autocorrelation function of the differential shimmer between light source a and light source b is

$$\phi_{a-b,a-b}(\tau) = \lim_{T\to\infty} \frac{1}{2T} \int [a(t)-b(t)][a(t+\tau)-b(t+\tau)]dt$$

$$= \lim_{T\to\infty} \frac{1}{2T} \left[\int a(t)a(t+\tau)dt + \int b(t)b(t+\tau)dt \right.$$

$$\left. - \int b(t)a(t+\tau)dt - \int a(t)b(t+\tau)dt \right] .$$

Therefore,

$$\phi_{a-b,a-b}(\tau) = \phi_{aa}(\tau) + \phi_{bb}(\tau) - \phi_{ba}(\tau) - \phi_{ab}(\tau) . \qquad (15)$$

If now the angular spacing of lights a and b is greater than the correlation angle, their shimmer is uncorrelated, and

$$\phi_{ab}(\tau) = \phi_{ba}(\tau) = 0 . \qquad (16)$$

Since also

$$\phi_{aa}(\tau) = \phi_{bb}(\tau),$$

it follows that

$$\phi_{a-b,a-b}(\tau) = 2\phi_{aa}(\tau) .$$

Thus the power density spectrum, which is the Fourier transform of the autocorrelation function, has the same form for differential shimmer of two uncorrelated sources as for the shimmer of one source about its mean position. The magnitude of each frequency components in $\Phi(\omega)$ is, however, twice as great for the differential shimmer, and hence the magnitude of $|A(\omega)|$, the shimmer spectrum, is itself greater by a factor $\sqrt{2}$, as seen from Equation (7).

Equation (16) presupposes no correlation between the apparent motion of the two light sources. Since we have lights at various spacings, we will, from the source-to-fiducial measurement of each source, be able to compute the crosscorrelation function $\phi_{ab}(\tau)$ of the angular displacements of each pair of lights. When the angular separation of such a pair of lights is great enough to cause the crosscorrelation function to vanish, we then compute $\phi_{a-b,a-b}(\tau)$, the autocorrelation function of the differential shimmer between them, and hence can obtain the spectral characteristics of the shimmer due to independent atmospheric turbulence. The effects of aircraft induced turbulence and residual vibrations are eliminated in the differencing process used to obtain $\phi_{a-b,a-b}(\tau)$. The data used are source-to-fiducial angular positions, but the differential source-to-source spacing is obtained by differencing the source-to-fiducial measurements of the two sources.

A more convenient, although less rigorous means of verifying that two light sources are sufficiently far apart to

be uncorrelated in their shimmer, is to compute the mean square power $\phi_{a-b,a-b}(0)$ of the differential shimmer, rather than the crosscorrelation function. As this process is repeated for lights at successively greater separations, the mean square differential shimmer power increases asymptotically to its maximum value, and levels off. When this point of leveling off is reached, the differential autocorrelation function $\phi_{a-b,a-b}(\tau)$ may then be computed to obtain the differential shimmer spectrum.

In any case, an additional output of these calculations (regardless of whether the vanishing of crosscorrelation or leveling off of mean shimmer power is used as a criterion) is the maximum correlation angle for the shimmer between two sources, which gives us information concerning the size and location of the "blobs," or cells, of turbulent air which are inducing the shimmer process (see Section 4.0 below). Thus we are able to find mean shimmer power, the shimmer spectrum, and the correlation angle of the shimmer, all duly corrected to remove the effects of vibration and aircraft turbulence.

2.2.2 Shimmer Resulting from Aircraft Induced Turbulence

It is desirable also to know how much of the total shimmer is actually due to aircraft induced turbulence. Since the calculation of Section 2.2.1 above has eliminated this effect, if we now compute the total shimmer as well, we can, by differencing the two results, obtain the extent of aircraft induced shimmer.

The total shimmer may be obtained by autocorrelating, not the difference between two apparent source positions, but rather the angular deviation a(t) of one source with respect to its mean position. The measurement process of course actually consists of source to fiducial measurement $a_f(t)$, but we have seen in Equation (14) above that this also obtains for us the spectrum of the movement with respect to mean position.

Unfortunately, however, when we observe the shimmer of a single source, we no longer cancel out the effect of residual aircraft vibrations, as we did for differential shimmer of two sources. In other words, when we eliminate vibrations we also eliminate aircraft induced turbulence, and when we include one we also include the other. Therefore, it is important in this measurement that aircraft vibrations have been sufficiently uncoupled from the photographic system so as to produce no significant effect on the results. Not only are we concerned about the aircraft vibration spectrum (as well as vibrations introduced by the camera itself), but also any beat frequencies between these components and those of the shimmer process we are observing.

The uncoupling of low frequencies is accomplished by the tracker platform servo, and the high frequencies are the responsibility of the vibration mount. To verify that what we are observing can be assigned to shimmer and not to vibration effects, various weights should be mounted on the camera in order to change its characteristic modes of vibration; the shimmer observation can be made at low altitudes, or perhaps on the

ground. Only if the observed shimmer spectrum is invariant under the change of camera vibration modes can we be assured that vibrations have actually been uncoupled.

The airborne measurement of total shimmer, and hence of aircraft induced turbulence, should be accomplished for at least two aircraft stations, corresponding to different induced turbulent environments, in order to obtain suitable information about this effect. Thus, in this experiment two cameras are mounted at different aircraft stations to make simultaneous measurements.

3.0 INSTRUMENTATION

It is proposed to utilize two high speed aircraft of any type typically used for tracker measurements. One is the target aircraft, the other is the observing aircraft. The target aircraft will be equipped with at least five high intensity narrow beam lamps spaced at intervals to provide a series of angularly spaced sources when viewed from the observing aircraft. The two aircraft will be separated at distances ranging from 10 to 50 kilometers.

The source spacing on the target aircraft will depend somewhat on the type of aircraft used; but a desirable configuration which will be used for instrument specification purposes would be five sources, four of which will be spaced in a horizontal line at distances of 1, 2, 4, and 8 meters from the fifth, or reference, source. At the maximum distance of 50 km., they will subtend .02, .04, .08, and .16 milliradians, respectively; at the minimum distance, 10 km., they will subtend 0.1, 0.2, 0.4, and 0.8 milliradians, respectively. These ranges and source intervals will provide a means of evaluating the shimmer effect as a function of distance, as well as allowing a comparison of the coherence of the shimmer motion as a function of angular separation.

The two aircraft will be constrained to fly on parallel courses at equal speed, but their altitudes can be varied to provide information about the effect of height and slant angle on

shimmer; the altitudes attainable are of course dependent on the type of aircraft used. However, the tropopause region of heavy turbulence, which is the expected source of the worst seeing effect problems, can be adequately covered by conventional aircraft, such as the KC-135.

The observing aircraft will be equipped with two high resolution telescopic cameras. The cameras will be individually shock mounted and stabilized against aircraft rotations, so as to be uncoupled from the aircraft vibration environment.

The size of the camera apertures is important to the basic experiment. Too large an aperture would modify the effects of shimmer by integrating the incoming wave fronts over a large area, and thus blur the image. Too small an aperture would confine the experiment by diffraction limiting the resolution, and by decreasing the film exposure. Therefore, a compromise figure of 20 cm. was set as the optimum aperture.

The data rate should be approximately three times the highest desired frequency (i.e., more than twice the highest frequency, in accordance with the Nyquist sampling criterion). From ground measured data, it has been established that the shimmer magnitudes drop to a low level above 100 hertz. Because the tracker will compensate for fluctuations below 10 hertz, it was decided to limit the experiment to frequencies between 10 and 120 hertz. Thus, the frame rate was set at approximately 360 frames/second, and at least 1 second of consecutive data (360 frames) should be taken during each measurement.

A tracking system will track the sources on the target aircraft and point the cameras with sufficient accuracy to keep the source images on the film format. Each frame will contain images of the five light sources and fiducial marks.

The primary information to be derived from the filmed data is the frame-to-frame fluctuations of the source images with respect to the fiducial. This will be done, at least for this initial experiment, by microdensitometer or microcomparator measurements on the developed film and will produce a time-varying amplitude record of the motion of these images. If there is a degree of coherence between the shimmer movements, as has been experienced by ground based telescopes, at small angular source separations, the differential shimmer between two sources will not be a measure of the shimmer of one source with respect to its mean position but will instead increase with increasing angular separation. When sufficiently large angles are encountered, the crosscorrelation between two source deviations should be zero and the differential shimmer should reach a maximum. Although no way has been found to predict at what angular separation the limit would be reached at these altitudes and speeds, it is believed that the range of separations provided in this experiment will include this maximum. This "saturation" amplitude becomes a measure of the shimmer when image distances have been related to angular dimensions by the optical geometry

$$\Delta\theta = \frac{\Delta x}{f} \quad ,$$

where

$\Delta\theta$ = angular dimension,

Δx = film linear dimension, and

f = focal length of the optical system.

From these data, then, will be produced a measurement both of differential shimmer between two sources as a function of angle, and the shimmer of one source alone. Both measurements will be free of mechanically induced vibration noise because of the fact that apparent image motion due to vibration will displace both sources equally.

Frame-to-frame fluctuations in the distance between a source image and a fiducial marker on the film will include all system noises, notably those produced by mechanical vibration. These noise signals must be kept low enough so that the shimmer-produced fluctuations are not masked. There will always be some noise of this type present, however, so that the magnitude of the source image to fiducial fluctuations will always be greater than those of the source image to source image measurements of differential shimmer. The difference between the magnitudes of the two fluctuations signals will be a good measure of the mechanical vibration of the camera and mount, as well as local shimmer due to aircraft induced turbulence, information which is not available for existing airborne telescopic cameras.

By providing a second camera, identical to the first, and synchronizing their frame rates, additional information can be derived. This will provide a comparison of shimmer amplitudes

(including aircraft induced turbulence) from two different positions on the aircraft simultaneously.

The method of reducing the data will be to take source image to fiducial distance fluctuation data from both cameras, and by means of a digital computer obtain differential shimmer and autocorrelation and crosscorrelation as needed.

3.1 Design Parameters

The important experiment parameters which affect instrument design have been discussed in the previous sections. They are tabulated as follows:

Data Rate - 360 Data Points per second,

Distance, Source to Target - 10 to 50 km,

Source Separation - 1, 2, 4, 8 meters, and

Receiver Aperture - 20 cm.

Figure 1 shows, in schematic form, how these experimental parameters affect the instrument design specifications of the sources and cameras. The details of the relationships between the boxes and the methods of determining each instrument parameter will be discussed in the following paragraphs.

3.2 Source Considerations

The source intensity should be as high as possible, commensurate with aircraft power availability and practical cooling methods. Increasing the source intensity makes possible faster frame rates, greater target distances and slower (thus higher resolution) film.

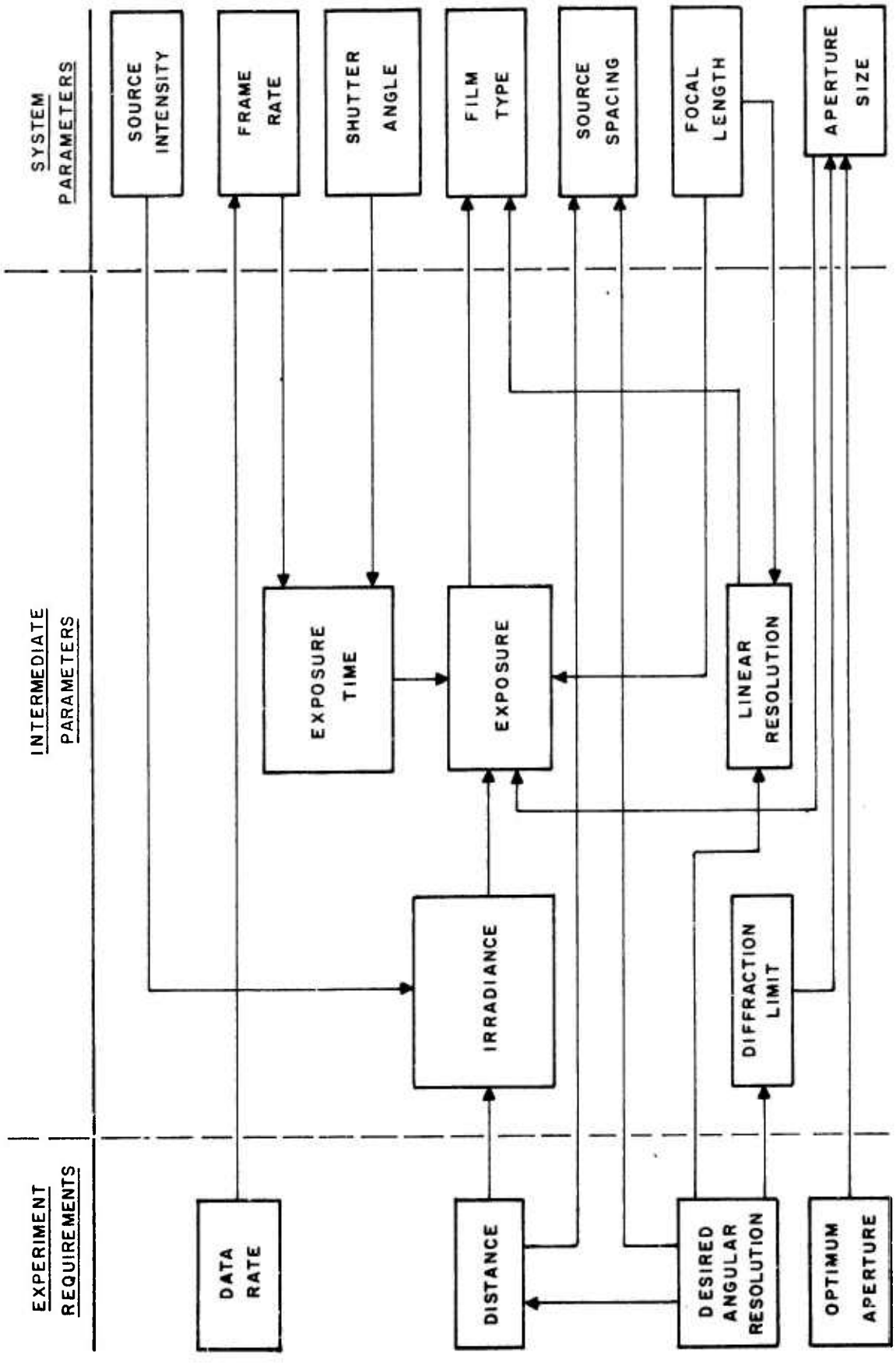

Figure 1. Instrument Design Relationships

Because of the photographic film used for this experiment, sources should have high intensity in the visible region of the spectrum. Two high powered light sources having the greatest output in this region and, at the same time, having good stability, are the Xenon Arc and the Tungsten Iodine lamps. These two lamp types are both being considered for use on this experiment. Choice will depend on a future analysis which should include aircraft power availability as well as a detailed cost analysis, including cost of power supplies, safety enclosures, etc. These considerations were felt to be beyond the scope of this report; instead, a brief description of each type will be included.

The Tungsten Iodine lamps are tungsten filament lamps which possess several characteristics which make them superior to conventional tungsten lamps. They do not blacken. The bulb remains perfectly clear until burnout because of the iodine cycle by which the evaporated tungsten is deposited back on the filament. The filament can be operated at a considerably higher temperature than conventional tungsten lamps, which of course means greater light producing efficiency. The lamps may be made much more compact for a given power rating than conventional lamps because the quartz envelope will withstand high temperatures. The stability of the lamps is so good that the 1000 watt type has recently been calibrated and used by the National Bureau of Standards as a standard of total irradiance. They are available from the General Electric Company with input power ratings between 45 and 1500 watts.

The Xenon Arc lamps are high pressure, high brightness light sources similar in principle to the more well-known Mercury Arc lamps. They have equivalent color temperatures on the order of 6000°K through the visible region of the spectrum.

Typical operating characteristics of 500 and 1000 watt Xenon Arc lamps are included and compared with a 1000 watt Tungsten Iodine.

	500W. Xenon	1000W. Xenon	1000W. TI
Rated Current (Amps)	28	45	54
Luminous Flux (Lumens)	12,750	42,000	32,000
Intensity (candles)		4,260	
Aug. Brightness cp/cm^2	35,000	60,000	
Conversion Efficiency		53%	
Luminous Efficiency (Lumens/watt)	25.5	42	32
Luminous Length	.150 inches	.150 inches	2.6 inches

As can be seen, the major differences between the Xenon and Tungsten lamps is the short luminous length, which is an advantage of the Xenon Arc lamp in that it produces a narrow beam. However, this advantage cannot be utilized to any extent because of considerations discussed in the next paragraph. The only major problem with the use of xenon is the high pressures (30 atmospheres) which is attained during use; this requires their being housed in appropriate enclosures.

Lamps of these types radiate into a very large solid angle. To use them efficiently for this experiment, they must be placed in an optical system which will direct their output into a narrow beam. The most used and most practical optical system for the purpose is a parabolic reflector with the lamp placed at its focal point. A perfect point source in such a system would produce a perfectly collimated beam. Any source will have a finite cross-sectional area, however, and this produced a beam divergence. Keeping this beam divergence small requires a small, intense source. If the increase of irradiance on a distant receiver due to directionalizing the beam is thought of as gain, as in an antenna, then the increase in gain produced by a parabolic reflector is approximately proportional to the ratio of reflector cross-sectional area to the source cross-sectional area.

There is a minimum limit, however, to the allowable beam width for this experiment, since the beam orientation is critical. Roll and yaw of target aircraft could cause the beam to miss the receiver unless each source were mounted on a stable platform, at great and unnecessary expense. A ten degree beam, a typical searchlight beam width, will still provide an intensity gain of approximately 100 and will remove the critical alignment problem between the aircraft which would obtain with the use of a narrower beam.

The ten degree beam is attainable by either Xenon Arc or Tungsten filament lamps and a 12" reflector. Therefore, the advantages of the small luminous area provided by the Xenon Arc

source cannot be utilized. For this reason, both types of lamps should be considered in the ultimate design.

The radiant power was calculated for a 1000 watt xenon lamp mounted in a parabolic enclosure to provide a 10° beam. The result was a radiant power of 100 watts/steradian between wavelengths 0.4 and 0.7 microns.

3.3 Camera Considerations

After choosing a source and determining its radiant power, the camera and film specifications can be considered. Camera and film cannot be separated, because the combination of the two together results in system sensitivity and resolution. The general approach is to look at available film emulsions and optical systems, noting the system relationships between them, and derive a combination which will produce the desired specifications.

3.3.1 Aperture

The aperture has been set by experimental requirements at approximately 20 cm diameter. This entrance diameter controls the absolute resolution limit of the optical system, since, by the Rayleigh criterion θ_a, the angular resolution of the system cannot be less than $1.22 \frac{\lambda}{D}$

where λ = wavelength of the incident radiation and

D = diameter of the aperture.

For 20 cm at 0.55 microns wavelength, θ_a = 3.4 microradians. This is much smaller than the required angular resolution. Therefore, the Rayleigh criterion will not be the limiting factor in our resolution.

3.3.2 Focal Length

The next engineering choice to be made is the selection of the focal length (f) of the optics. This length transforms the linear resolution (LR) at the film plane to angular resolution (θ_R),

where

$$\theta_R = \frac{LR}{f}$$

for small angles.

The focal length must be made long enough so that film resolution does not limit the system, and short enough so that image intensity is great enough to expose the film in the fixed time of exposure. The film resolution power has been determined to be approximately 100 lines/mm. To utilize this resolution and to provide .005 mr (1 arc second) angular resolution for the camera lens requires a 2,000 mm focal length. Source and film considerations to be discussed next indicate that this is a sound choice from the standpoint of film sensitivity. A later section will show that cameras having similar focal lengths are in use, and obtain resolutions of approximately this value, often under more adverse conditions.

3.4 Film Exposure

The individual lamp sources will be unresolved in the film plane. This means that the spot size on the film in the receiver will be unrelated to source size, but will be related to film characteristics and lens resolution characteristics. The design objective of 100 lines/mm resolving power for the camera results in a spot size of approximately 0.01 mm, depending on the type of film used, its exposure and developing conditions, and lens aberrations. The radiant power entering the camera aperture will then be distributed over an area approximately 10^{-6} cm^2. H_R, the radiant power at a distance of 50 km, will be 2×10^{-12} watts/cm^2, assuming an atmospheric extinction of 50% which is a very conservative estimate for typical conditions at the altitudes to be used. This will produce an irradiance on the film, assuming no lens losses, of

$$H_f = H_R \frac{A_{aperture}}{A_{spot}} = 8 \times 10^{-4} \text{ watts/cm}^2.$$

The film exposure, E, is related to the film irradiance by

$$E = 10^7 H_f t \text{ ergs/cm}^2 ,$$

where t is the time of exposure in seconds; hence, for an exposure time of $\frac{1}{1000}$ sec,

$$E = 8 \text{ ergs/cm}^2.$$

Selection of film sensitivity is now possible.

3.5 Film Type

Film type is the next item to be examined. In considering film, both resolution and sensitivity must be considered. Films chosen must be available on Estar base for use in cine cameras of 16 or 35 mm types. Upon examination of several film types, it was decided that Kodak Plus-X Aerographic film combines the attributes of high sensitivity, wide spectral range, and good resolution. The resolving power at T.O.C. 1000:1 is 100 lines/mm. It has a log sensitivity of 1 to produce a density of 1.0 over its entire spectral range from 0.4 to 0.7 microns. This means an exposure of 0.1 ergs/cm^2 will produce the given density.

3.6 Film Dimensional Instability

The film limitations for this measurement program are closely related to those involved in aerial mapping. The most important limitation is dimensional stability, which refers to the ability of film to retain its exact shape under the various chemical environments, temperature, and mechanical stresses to which it is subjected during exposure, development, and readout.

Dimensional instability is of prime importance to this program, because the information taken from the film is primarily dimensional. Fortunately, this property of film has been quite extensively studied, and film bases have been developed to minimize these instabilities. In the following paragraphs, the various

causes of dimensional instability will be reviewed and approximate values will be given.

The dimensional changes which occur in film have a variety of causes. Some of these changes are of a temporary nature and others are permanent. Temporary changes are caused by expansion and contraction of the film due to changes of temperature and humidity. Permanent changes are caused by processing and aging effects, and by mechanical stresses placed on the film during exposure.

Dimensional changes will be divided for our purposes into two types. Those which occur uniformly over the entire film area will be called scale distortions, and those which effect only a small part of the film will be termed local distortions.

The largest distortions are scale distortions which are uniform over the entire film area. They cause a scale change on the film which is, at worst, only a few hundredths of a percent for Estar base films. Frame-to-frame scale changes can be calculated out in data reduction with the placement of two or more fiducial marks on each frame by means of fiducial markers in the cameras. Dimensions on the film can then be normalized to the distance between these fiducial marks. This will reduce frame-to-frame error to the level of local distortions.

Local distortion is the item of greatest concern, because this contributes errors directly to the dimensional data taken from the film.

An important study [3-1] of film dimensional changes has been made by Eastman Kodak using their Super XX Aerographic film type 5425 (cellulose acetate-butyrate base) and Kodak Double-X Aerographic film, type 2404 (Estar base). For this study, rolls 180 and 230 feet in length respectively were used. The process consisted of contact exposing the film to a glass plate containing a uniform 300-line, 50% halftone image. After photographic processing, the film is registered with another halftone image on a glass plate. This registration of two halftones with different dot spacings creates a moiré pattern in which change in the relative position of the moiré cancellations denotes a change in the film dimensions between the time of exposure and registration. This can be calculated knowing the halftone spacing and the spacing between moiré cancellations. The films were exposed over their entire length and sent to six different commercial processing laboratories for development. Results of the tests were as follows:

Estar base films showed a definite advantage over cellulose acetate-butyrate base films, both in having lower scale distortions and smaller local distortions. Estar base films also showed less variation in results from different processing plants, which indicates that environmental conditions are not as critical for this type of film. Processing must be carefully watched even for the Estar base films, however. Local distortions can be caused by uneven heat or humidity of the film during exposure or readout. Care must be taken that water droplets are not left on the

emulsion surface during drying. The film must not be subjected to excessive tensions, and adequate time must be allowed for drying after processing and for moisture conditioning prior to printing. Under the best conditions, for Estar base films, local distortion averages between 0.005 and 0.01 mm, which is the average of the displacement of point images on the film over a 9" square frame.

3.7 Image Motion Blur

Image motion blur is caused by relative motion between the target and the optical axis of the telescope during the exposure period. To minimize this target motion, the product of the angular velocity of the tracking system and the exposure period must be smaller than the angular resolution required of the system, which we have set at .005 milliradians. The maximum ω allowed for this condition is 5 milliradians/second.

Because the aircraft involved in the experiment are flying parallel courses at identical speed, and at large distances, their angular relationship will not change appreciably, and their relative angular velocity will be essentially zero. Angular changes, compensated by the tracker, will occur as the receiver aircraft changes in roll and yaw. Roll and yaw rms rates have been measured for typical tracking aircraft and do not exceed 5 milliradians/second. Because of tracker compensation for these movements, the rates shall be considerably reduced from this figure. Therefore, this source of possible blurring has also been rejected.

Other possible sources of image blurring are camera induced vibration, aircraft induced vibration and very high frequency shimmer. The camera induced vibration limit should be a specification on camera selection. Aircraft induced vibration should be damped out by proper mounting. Both must be held below the 5 mr/sec. level.

3.8 Camera Selection

The camera format size has to be large enough so that the target is always held within the field of view of the camera. With a 2,000 mm focal length lens, a 16 mm format provides a 5.2 milliradian field, while a 35 mm format provides a 12.4 milliradian field. Either size would be well within the capabilities of most trackers with proper boresighting and calibration. The camera requirements, determined previously, are frame rate, approximately 360, exposure time, approximately .001 second, and overall resolution, greater than 100 lines/mm.

In search of available cameras, the one which appeared most applicable was the Photosonics 35 mm 4E. This camera is vacuum backed, has 4-pin registration and 12 pull-down claws. It has a maximum frame rate of 360 frames per second with a 120° shutter, so that the exposure period would be $\frac{1}{1080}$ second. Time markers and fiducial markers can be provided for this camera.

3.9 Existing Camera Systems

A brief description of three camera systems presently in use is included here for information purposes and may be used as possible sources of further information or as a basis for acquisition of camera equipment. It shall also serve to demonstrate that camera requirements for this experiment are not beyond the state-of-the-art.

The Northrop Nortronics ALOTS (Airborne Lightweight Optics Tracking System) uses a 70 mm camera to provide sequential photographic coverage; this camera is a modified Photosonics Model 10-A which produces 2 1/4" x 2 1/4 " photographs at up to 80 frames per second. Camera telescope optics consist of a 200-inch focal length T/16 system with primary and secondary reflecting elements, a Schmidt type correcting plate placed in front of the reflecting elements, and an air spaced doublet lens and field flattener placed in the converging beam close to the focal plane. The system field of view is 55 minutes. Focus control from 5 miles to infinity is achieved by a remotely controlled optical wedge. With this camera tracker system, resolution of less than 2 seconds was obtained on 70% of the frames while flying at normal cruising speed from 40,000 ft. altitude, to the ground, in light turbulence. The dynamic slaving accuracy is 5 arc minutes.

Lincoln Laboratory uses a 100" focal length Ranson Laboratories 14" diameter 70 mm camera with frame rates of 6 or 60 frames per second. This camera has 2 arc second resolution. Time is recorded on one side of the frame in IRIG B format, and on the

other side a set of neutral density wedges and a data box are recorded. The field of view of the camera is 27.5 minutes on a 70 mm format.

AVCO Corporation uses a 2,000 mm telescope of their own design which uses a modified Cassegrain optical system. Their optical system design has the following parameters:

Primary Mirror - Parabolic - 4% overcorrected to eliminate 3rd order coma
- 36" radius of curvature
- 7.5" optical element diameter
- 6.2" effective diameter

Secondary Mirror - Hyperbolic - 4% overcorrected to eliminate 3rd order coma, figured to eliminate on-axis spherical aberration
- 10" nominal radius of curvature
- 1.9" optical element diameter
- 1.6" effective diameter

It achieves a 0.3° field of view with a 35 mm format; the camera was a Mitchell GC capable of framing at 120 frames/second with a 15° shutter.

3.10 Tracker Considerations

The purpose of the tracker is to position the cameras so that the target is continuously in the field of view; the tracker will, therefore, lock onto the light sources being photographed by the cameras.

For a tracker to successfully track this target (Section 3.0) it must stay locked on the entire source cluster; thus its angular resolution should be in the order of one milliradian. [It should not have poorer resolution than this because of the essential purpose of keeping the camera positioned on the target within its field of view; its angular resolution, therefore, should be approximately one to two milliradians.] Its response time has been set by experimental requirements at 5 to 10 cps. Its NEDP must be less than 1/20 of the total irradiance from the six sources when they are at the maximum distance of 50 km. This amounts to 6×10^{-13} watts/cm^2. These are not difficult tracker specifications, providing the sensor used is a photomultiplier. Any one of several tracking systems could be used.

In keeping with the non-classified nature of this volume, tracker parameters will not be discussed, but the reader is referred to reference [3-2], a recent survey of available tracking systems by the Lowell Technological Institute Research Foundation. Unclassified specifications for a tracker which could be used are included here; it is the Barnes Engineering Company Model 21-122. The P-M channel only would be used. The specifications of this tracker are:

Optical System Resolution	Folded-Reflecting Telescope
Field of view	1° x 1°
Aperture	8 inch
Effective Aperture due to obscuration (diameter)	7.2 inch
Focal Length	50.0 inch
Focal Ratio (Geometric)	f/5
Focal Ratio (with immersion lens)	f/1.0
Focus Range	34 ft. to Infinity
Crossover Wavelength	0.65μ
Dichroic beam-splitter	90% Reflective to wavelengths shorter than 0.56μ
	90% Transmissive to wavelengths longer than 0.78μ

Field Lens System	
P-M Channel, 2-Element	Glass
PbS Channel, single element	Arsenic trisulfide

Detector Assembly	
Infrared (Channel 1)	Uncooled, lead sulfide, Strontium titanate immersed
Spectral Range	0.7-2.8μ (0°C)
NEPD	1.5×10^{-12} watts/cm^2
Photomultiplier (Channel 2)	Nine stage photomultiplier
Spectral Range	0.35 - 0.56μ
NEPD	1.6×10^{-16} watts/cm^2

Electrical Signals

Azimuth Transfer Function	2500 Volts/radian (adjustable)
Elevation Transfer Function	2500 Volts/radian (adjustable)
Zero Drift	Not more than ±200 mv/5 hrs.

Power Required

Operating Voltage	115± 5 volts
Frequency	400± 20 cps
Consumption	140 V.A.
D.C. Power (28 Volts)	0.15 Amp.

4.0 APPENDIX-DISCUSSION OF THEORETICAL MODELS

4.1 Seeing Effects

When a distant source is observed with a telescope of small aperture and long focal length, the image, instead of being steady, appears to fluctuate both in position and intensity. These effects are known as seeing effects. While many names are used in the literature to describe this effect, the most common usage and the ones adopted for this report are as follows:

Scintillation - refers to the variation of intensity of the light reaching the telescope.

Shimmer - refers to the image movement, caused by atmospheric effects, in three dimensions. Shimmer has been subdivided into two-dimensional movements in the focal plane, known as agitation, and extra-focal movements, known as defocussing.

All of these phenomena are due to irregularities of various dimensions and at various heights above the ground in the structure of the atmosphere.

This experiment is primarily centered on the agitation part of the shimmer effect, the two-dimensional movements of the target image.

As observed from the ground, at least two distinct regions of refractive anomalies in the atmosphere play a role in scintillation and shimmer. These are the tropopause region and the region near the ground. It is generally agreed that for ground based telescopes scintillation is caused by anomalies in

the upper atmosphere whereas near-ground turbulence causes shimmer effects.

In a fast-moving aircraft at high altitudes, the conditions are quite different, because the telescope is now moving at a rapid rate through a turbulent field that is quite different from that experienced by the ground based apparatus. For this reason, models of turbulence affecting shimmer on the ground have little application, and further, sufficient data are lacking on upper atmospheric turbulence to attempt a model at this time. However, a few assumptions have been made on the nature of the turbulence, and will be discussed briefly. The effect of this turbulence on the optical system is now considered, as well as a possible means for using the data produced by this experiment to contribute to knowledge of this atmospheric turbulence.

4.2 Atmospheric Turbulent Cells

A study of the causes of shimmer must include a study of the shape, size, and motion of atmospheric anomalies, or as named by Zwicky [4-1], "aerial blobs". These blobs, according to Zwicky and others, are reasonably stable atmospheric anomalies which tend to hold their size and shape for periods at least of the order of minutes. To quote from Zwicky, "Although many atmospheric disturbances refract, diffract, scatter, or absorb light from celestial and terrestrial sources in an irregular manner, there exists evidence for volumes of air of locally altered density,

temperature, and water content that possess remarkable properties. Blobs in combination with the mirrors or lenses of a telescope often bodily displace the images of stars or focus them in points in front or behind the regular focal surface, ..."

These aerial blobs essentially behave like a system of random lenses of odd shapes. If these turbulent cells are represented by hot air parcels of lower density and lower index of refraction than the ambient air passing along in front of the telescope objective, they behave like divergent lenses. If the ambient air is warmer than the temperature of the parcels, they would behave as convergent lenses.

4.3 Size of the Turbulent Cells

Assuming that the blob theory is a useful analogy, some information can be derived from the experimental shimmer data to determine the blob size, as follows:

The angular size that the blobs subtend, as seen from the aircraft, can be determined by examining the variation in differential shimmer as the angle between sources is increased at a fixed target range. The correlation of the source fluctuations is a measure of the angular size of the blobs. Therefore, on a statistical basis, a model of the blob angular size range can be generated for the various altititude and sighting angles through which the aircraft flies. Eventually, more extensive data obtained in later, more elaborate, experiments could

conceivably lead to estimates of the effective range of the primary shimmer-producing blobs, and hence of their actual dimensions, based, perhaps, on triangulation from multiple aircraft stations.

4.4 Hosfeld's Experiment

Because of its direct applicability to the proposed experiment, a description of an important measurement of shimmer taken by a ground based telescope is included. It is directly quoted from Hosfeld [4-2], who observed the shimmer of double stars.

"A distinction between the characteristics of image motion and scintillation becomes apparent when the behavior of double stars is examined. If the intensity changes suffered by the two components are in phase, it follows that the percent scintillation will be the same whether the components are observed singly or together. If, however, the scintillation is incoherent, some mutual cancellation of intensity changes will occur, resulting in reduced percent scintillation for the pair. The double star θ Serpentis, whose components are sufficiently separated (20 seconds of arc) to be measured individually, gave less percentage variation when both components were measured than when only one was measured. Even the much closer double star Castor, 2.6 seconds of arc separation, showed reduced scintillation when compared to a single star, Pollus, at the same elevation angle.

Thus we conclude that the scintillation of double star components of this separation is largely incoherent.

On the other hand, that the motion of the images of the components of these double stars is coherent was observed in the following manner: A cardboard diaphragm with two 3-inch apertures, separated by 9 inches, center to center, was placed over the telescope objective. When the focal plane of the eyepiece was displaced somewhat from the focal plane of the telescope four images were observed, since each aperture formed an image of the double star. Let A and B be the components of the double star, and I and II be the objective diaphragm apertures. Then, A_I represents the image of component A formed by aperture I, B_I represents the image of component B formed by aperture I, etc. (see Fig. 2). An examination of the quadrilateral formed by these extrafocal images revealed that the sides A_IA_{II} and B_IB_{II} are of variable length, while the sides A_IB_I and $A_{II}B_{II}$ remain unchanged in length and constant in direction.

In short, two closely spaced apertures form images of a single star which move independently, but a single aperture forms images of two closely spaced stars which move together, or coherently. Such <u>coherent motion</u> of the images of the components of double stars is in direct contrast to the <u>incoherent</u> scintillation of the components."

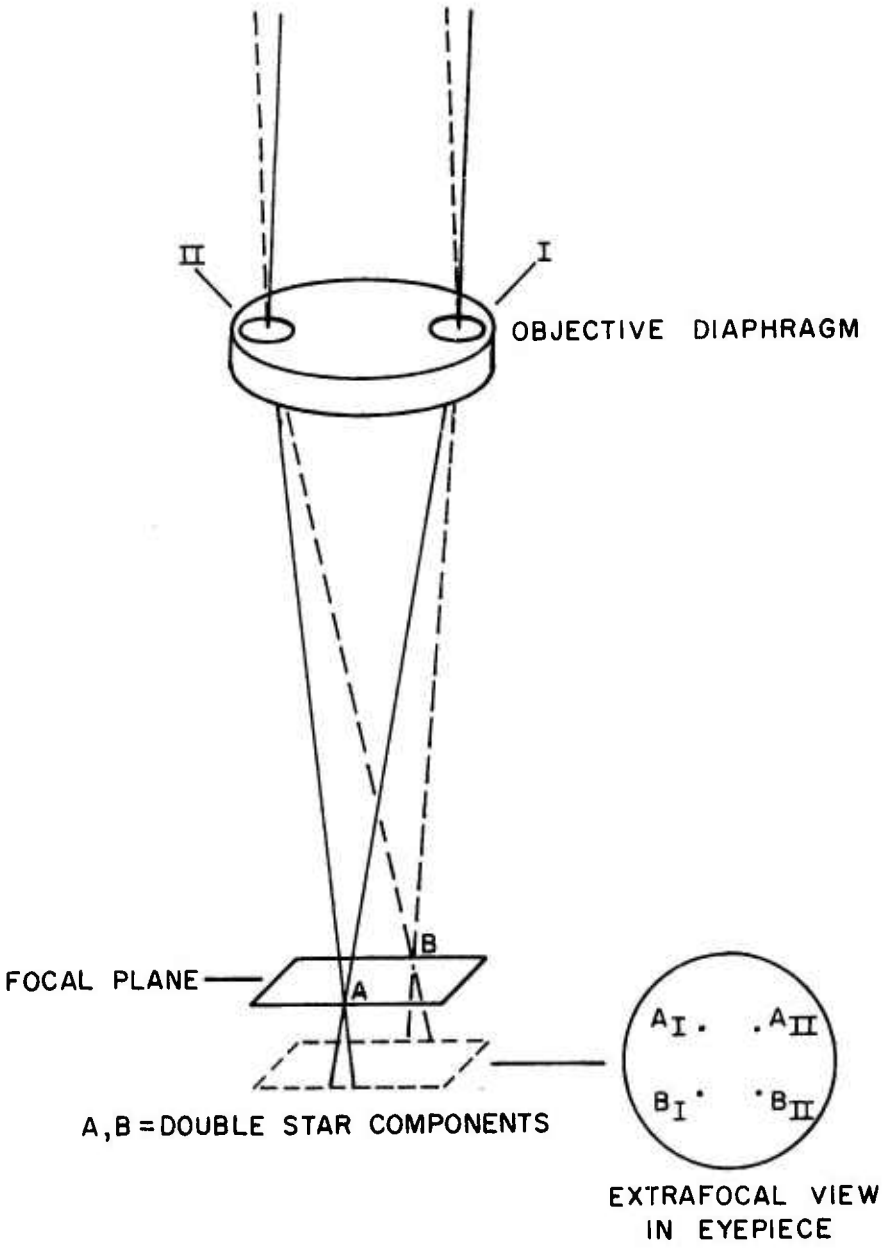

Figure 2. Hosfeld's Experiment

5.0 REFERENCES

[2-1] Lee, Y.W., Statistical Theory of Communication, John Wiley and Sons, p. 36 (1960).

[3-1] Adelstein, P.Z., Josephson, P.R., and Leister, D.A., "Nonuniform Film Deformational Changes," Photogrammetric Engineering, pp. 1028-1034, November 1966.

[3-2] "Study of Cost Relationship vs Tracking Accuracy of Airborne Infrared Trackers (U)," Vol. I and II (Secret), Contract No. AF33(615)-3120, Final Technical Report, December 1965.

[4-1] Zwicky, F., "Aerial Blobs," Science 122, pp. 159-160 (1965).

[4-2] Hosfeld, R., "Comparisons of Stellar Scintillation with Image Motion," J. Opt. Soc. Am. 44, pp. 284-288 (1954).